Maximum entropy analytic continuation of anomalous self-energies

Changming Yue [1,2,*] and Philipp Werner [1,†]

[1]*Department of Physics, University of Fribourg, 1700 Fribourg, Switzerland*
[2]*Department of Physics, Southern University of Science and Technology, Shenzhen 518055, China*

The anomalous self-energy plays an important role in the analysis of superconducting states. Its spectral weight provides information on the pairing glue of superconductors, but it can change in sign. In many numerical approaches, for example, Monte Carlo methods based on the Nambu formalism, the anomalous self-energy is obtained on the Matsubara axis, and nonpositive spectral weight cannot be directly obtained using the standard maximum entropy analytic continuation method. Here, we introduce an auxiliary self-energy corresponding to a linear combination of the normal and anomalous self-energies. We analytically and numerically prove that this auxiliary function has non-negative spectral weight independent of the pairing symmetry, which allows to compute the sign-changing spectrum of the original self-energy using the maximum entropy approach. As an application, we calculate the momentum-resolved spectral function of K_3C_{60} in the superconducting state.

DOI: 10.1103/PhysRevB.108.L220503

Introduction. The anomalous self-energy $\Sigma^{ano}(\mathbf{k}, \omega)$, defined in the Gor'kov-Nambu formalism [1,2], with $\mathbf{k}$ the crystal momentum and ω the real frequency, plays a crucial role in the theory of superconductivity. It is proportional to the superconducting gap function $\Delta(\mathbf{k}, \omega)$ [3], which provides information on the spatial and dynamic structure of Cooper pairing. The spatial structure, encoded in the $\mathbf{k}$ dependence of Σ^{ano}, determines the pairing symmetry as s, p, d wave, etc. The static value $\Sigma^{ano}(\mathbf{k}, 0)$ measures the strength of pairing, the high-frequency limit $\Sigma^{ano}(\mathbf{k}, \infty)$ is proportional to the superconducting order parameter Δ, and the ratio $\Sigma^{ano}(\mathbf{k}, 0)/\Delta$ defines the effective attractive interaction [4]. The Cooper pairing in realistic superconductors is retarded. The retardation in conventional superconductors comes from the coupling to phonons, but shows up in the frequency-dependent electron self-energy [5–11]. In unconventional superconductors, the retardation originates from other types of excitations, such as spin [12,13], orbital [4,14,15], or nonlocal magnetic fluctuations [16–19]. The retardation effect is described by the frequency-dependent gap function, the calculation of which is closely related to that of $\Sigma^{ano}(\mathbf{k}, \omega)$. Obtaining the real-frequency Σ^{ano} is thus essential for understanding the properties of superconductors and in particular the pairing mechanisms.

The retarded nature of the pairing can be experimentally measured. For example, the frequency dependence of the local gap function can be measured in scanning tunneling microscopy (STM) experiments [20–22]. In the last two decades, the development of laser angle-resolved photoemission spectroscopy (laser ARPES) [23,24] made it feasible to extract $\Sigma^{ano}(\mathbf{k}, \omega)$ and hence the gap function or pairing Eliashberg function with high momentum and frequency resolution

[25,26]. Machine learning techniques have also recently been used to extract $\Sigma^{ano}(\mathbf{k}, \omega)$ from ARPES data [27].

In numerical simulations of superconducting states, the normal and anomalous self-energies are usually obtained as a function of imaginary time or Matsubara frequency $i\omega_n$. Analytic continuation from the imaginary axis $(i\omega_n)$ to the real-frequency axis $(\omega + i\eta)$ is needed to obtain the real-frequency self-energy. In Migdal-Eliashberg studies of conventional phonon-mediated pairing, Σ^{nor} and Σ^{ano} can be obtained on the Matsubara axis with high numerical accuracy, so that the Padé approximation can be used for the analytic continuation [28]. Dynamical mean-field theory (DMFT) [29–33] and its cluster extensions [34–40] in the Gor'kov-Nambu formalism can be used to explore the typically unconventional superconducting states of strongly correlated electron systems. These methods map the interacting lattice system in the superconducting state to a self-consistently determined quantum impurity model with a superconducting (SC) bath. Such an impurity model with a SC bath can be solved with the exact diagonalization (ED) method [16,41,42] directly on the real-frequency axis, circumventing the problem of analytical continuation [43–45]. However, ED impurity solvers can only treat a limited number of impurity and bath orbitals, which results in spiky spectra of the gap function or self-energy.

Quantum Monte Carlo (QMC) methods provide a more accurate description of the unconventional pairing state on the Matsubara axis [38,46–53]. However, since QMC results contain noise in the Green's functions and self-energies, the Padé approximation, which is not robust against noise, can become unreliable. This method also does not ensure the positive spectral weight of the normal self-energy. The maximum entropy (MaxEnt) method [54] is a more robust and widely used method for the continuation of noisy numerical results, but its direct application is limited to functions with a positive definite spectrum. Unfortunately, the spectral weight of Σ^{ano}

*yuecm@sustech.edu.cn
†philipp.werner@unifr.ch

generally has sign changes on the real axis and thus MaxEnt cannot be directly applied.

An auxiliary gap function $\tilde{\Delta}(i\omega_n) = [\Delta(i\omega_n) - \Delta(i0^+)]/(i\omega_n)$, which is odd in ω_n, was introduced in Ref. [3] and it was assumed that the spectral weight $-\mathrm{Im}\,\tilde{\Delta}(\omega + i\eta)$ is positive. However, ED results (e.g., Fig. 1 in Ref. [43]) and the simple model systems treated below show that sign changes may appear in $-\mathrm{Im}\,\Delta(\omega + i\eta)$ and hence $-\mathrm{Im}\,\tilde{\Delta}(\omega + i\eta)$. In the case of particle-hole symmetric systems, one can introduce and analytically continue an auxiliary self-energy $\Sigma_\pm = \Sigma^{\mathrm{nor}} \pm \Sigma^{\mathrm{ano}}$ with non-negative spectral weight [55], but this method does not apply to particle-hole asymmetric systems, such as cuprates with realistic band structures, or the fulleride compound K_3C_{60} studied in this Letter. Reymbaut *et al.* [56] proposed the so-called MaxEntAux method, where MaxEnt is applied to a properly defined auxiliary Green's function for a particle-hole mixed operator with positive-definite spectral weight $\mathcal{A}^{\mathrm{aux}}(\mathbf{k}, \omega) \geqslant 0$. In this method, the spectral function of the anomalous Green's function $\mathcal{A}^{\mathrm{ano}}(\mathbf{k}, \omega)$ can be extracted as $\mathcal{A}^{\mathrm{ano}}(\mathbf{k}, \omega) = \frac{1}{2}[\mathcal{A}^{\mathrm{aux}}(\mathbf{k}, \omega) - \mathcal{A}_\uparrow(\mathbf{k}, \omega) - \mathcal{A}_\downarrow(\mathbf{k}, -\omega)]$, where $\mathcal{A}(\omega)$ is the normal spectral function. By using the Dyson equation, one can obtain from this the spectral function of the normal and anomalous self-energy, *if* the normal interorbital components of the lattice Green's function vanish. However, many realistic systems do not satisfy this condition for generic $\mathbf{k}$. Also, to get the $\mathbf{k}$-resolved spectral function or optical conductivity in the SC state, one has to perform MaxEntAux for each $\mathbf{k}$ point, which is more time consuming than performing the analytic continuation of the self-energy, especially when the self-energy can be assumed to be local or restricted to a small cluster.

Auxiliary self-energy. The self-energy of an interacting system, local or nonlocal, can be reproduced by an auxiliary noninteracting Hamiltonian [57–59]. This is achieved by connecting noninteracting bath sites to the sites of the lattice. The frequency dependence or retardation of the self-energy is mimicked by the hopping between the bath and lattice sites. (Note that this auxiliary bath is different from the effective bath of the DMFT impurity model, which represents the lattice environment.) Such an auxiliary model Hamiltonian is also used in the hidden fermion theory [44], where the c electrons are the electrons of the system and the f electrons (hidden fermions) are those of the auxiliary bath sites. The self-energy of the interacting system can be obtained by integrating out the f degrees of freedom. In the SC state of the interacting system, the hidden fermion model reads [44]

$$
\begin{aligned}
H_{cf} = \sum_{\mathbf{k}\sigma} &\left\{ [\epsilon_c(\mathbf{k}) + s(\mathbf{k})]c_{\mathbf{k}\sigma}^\dagger c_{\mathbf{k}\sigma} + \sum_\alpha \epsilon_{f_\alpha}(\mathbf{k}) f_{\alpha\mathbf{k}\sigma}^\dagger f_{\alpha\mathbf{k}\sigma} \right\} \\
&+ \sum_{\mathbf{k}\sigma\alpha} V_\alpha(\mathbf{k})(f_{\alpha\mathbf{k}\sigma}^\dagger c_{\mathbf{k}\sigma} + \mathrm{H.c.}) \\
&- \sum_{\mathbf{k}} D_c(\mathbf{k})(c_{\mathbf{k}\uparrow} c_{-\mathbf{k}\downarrow} + \mathrm{H.c.}) \\
&- \sum_{\alpha\mathbf{k}} D_{f_\alpha}(\mathbf{k})(f_{\alpha\mathbf{k}\uparrow} f_{\alpha-\mathbf{k}\downarrow} + \mathrm{H.c.}),
\end{aligned}
\tag{1}
$$

where $\epsilon_c(\mathbf{k})$ and $\epsilon_{f_\alpha}(\mathbf{k})$ are the bare dispersions of the c and f fermions, while $D_c(\mathbf{k})$ and $D_{f_\alpha}(\mathbf{k})$ represent the pairing strength between the c and f fermions, respectively. The pairing symmetry is encoded in the $\mathbf{k}$ dependence of $D_c(\mathbf{k})$ and $D_{f_\alpha}(\mathbf{k})$. The hybridization between the c and f fermions is denoted by $V_\alpha(\mathbf{k})$, while $s(\mathbf{k})$ represents the high-frequency limit of the normal self-energy (see below). In Eq. (1), we consider the one-band case for the c fermions.

Let us introduce the notations $\omega^+ \equiv \omega + i\eta$ [$(-\omega)^+ \equiv -\omega + i\eta$] with $\eta = 0^+$. By integrating out the f degrees of freedom, one obtains the normal and anomalous self-energy of the c fermion as

$$
\Sigma_{\mathbf{k}}^{\mathrm{nor}}(\omega^+) = s(\mathbf{k}) + \sum_\alpha \frac{|V_\alpha(\mathbf{k})|^2[\omega^+ + \epsilon_{f_\alpha}(\mathbf{k})]}{(\omega^+)^2 - \epsilon_{f_\alpha}(\mathbf{k})^2 - D_{f_\alpha}(\mathbf{k})^2}, \tag{2}
$$

$$
\Sigma_{\mathbf{k}}^{\mathrm{ano}}(\omega^+) = D_c(\mathbf{k}) + \sum_\alpha \frac{-|V_\alpha(\mathbf{k})|^2 D_{f_\alpha}(\mathbf{k})}{(\omega^+)^2 - \epsilon_{f_\alpha}(\mathbf{k})^2 - D_{f_\alpha}(\mathbf{k})^2}. \tag{3}
$$

The derivation of these expressions is provided in Appendix A of Ref. [44]. $s(\mathbf{k})$ [$D_c(\mathbf{k})$] is the frequency-independent part of the normal (anomalous) self-energy. Obviously, the poles of $\Sigma_{\mathbf{k}}^{\mathrm{nor}}$ and $\Sigma_{\mathbf{k}}^{\mathrm{ano}}$ are located at the same energies $\omega_{\mathbf{k}} = \pm\sqrt{\epsilon_{f_\alpha}(\mathbf{k})^2 + D_{f_\alpha}(\mathbf{k})^2}$.

We now define the auxiliary self-energy in the Matsubara frequency space as the following linear combination of the normal and anomalous self-energy,

$$
\begin{aligned}
\Sigma_{\mathbf{k}}^{\mathrm{aux}}(i\omega_n) &= \Sigma_{\mathbf{k}}^{\mathrm{ano}}(i\omega_n) + \frac{\Sigma_{\mathbf{k},\uparrow}^{\mathrm{nor}}(i\omega_n) - \Sigma_{\mathbf{k},\downarrow}^{\mathrm{nor}}(-i\omega_n)}{2} \\
&= \Sigma_{\mathbf{k}}^{\mathrm{ano}}(i\omega_n) + i\,\mathrm{Im}\,\Sigma_{\mathbf{k}}^{\mathrm{nor}}(i\omega_n),
\end{aligned}
\tag{4}
$$

where in the second step a paramagnetic state is assumed with $\Sigma_{\mathbf{k},\uparrow}^{\mathrm{nor}} = \Sigma_{\mathbf{k},\downarrow}^{\mathrm{nor}} = \Sigma_{\mathbf{k}}^{\mathrm{nor}}$.

The real-frequency auxiliary self-energy of the paramagnetic state thus reads

$$
\begin{aligned}
&\Sigma_{\mathbf{k}}^{\mathrm{aux}}(\omega^+) \\
&= \Sigma_{\mathbf{k}}^{\mathrm{ano}}(\omega^+) + \frac{\Sigma_{\mathbf{k}}^{\mathrm{nor}}(\omega^+) - \Sigma_{\mathbf{k}}^{\mathrm{nor}}(-\omega^+)}{2} \\
&= \mathrm{Re}\,\Sigma_{\mathbf{k}}^{\mathrm{ano}}(\omega^+) + \frac{\mathrm{Re}\,\Sigma_{\mathbf{k}}^{\mathrm{nor}}(\omega^+) - \mathrm{Re}\,\Sigma_{\mathbf{k}}^{\mathrm{nor}}[(-\omega)^+]}{2} \\
&\quad + i\,\mathrm{Im}\,\Sigma_{\mathbf{k}}^{\mathrm{ano}}(\omega^+) + i\frac{\mathrm{Im}\,\Sigma_{\mathbf{k}}^{\mathrm{nor}}(\omega^+) + \mathrm{Im}\,\Sigma_{\mathbf{k}}^{\mathrm{nor}}[(-\omega)^+]}{2},
\end{aligned}
\tag{5}
$$

where the property $\Sigma_{\mathbf{k}}^{\mathrm{nor}}(-\omega^+) = [\Sigma_{\mathbf{k}}^{\mathrm{nor}}(-\omega)^+]^*$ has been used.

The auxiliary self-energy corresponding to Eqs. (2) and (3) has positive definite spectral weight. A straightforward derivation [see Supplemental Material (SM) [60]] gives

$$
\begin{aligned}
&\mathrm{Im}\,\Sigma^{\mathrm{aux}}(\omega + i\eta) \\
&= -\sum_\alpha |V_\alpha(\mathbf{k})|^2 \eta \\
&\quad \times \frac{(\omega - D_{f_\alpha}(\mathbf{k}))^2 + \eta^2 + \epsilon_{f_\alpha}(\mathbf{k})^2}{[\omega^2 - \eta^2 - \epsilon_{f_\alpha}(\mathbf{k})^2 - D_{f_\alpha}(\mathbf{k})^2]^2 + 4\omega^2\eta^2} < 0,
\end{aligned}
\tag{6}
$$

which yields $A_\Sigma^{\mathrm{aux}}(\omega) = -\mathrm{Im}\,\Sigma^{\mathrm{aux}}(\omega + i\eta)/\pi > 0$. Hence, the auxiliary self-energy defined in Eq. (4) has positive spec-
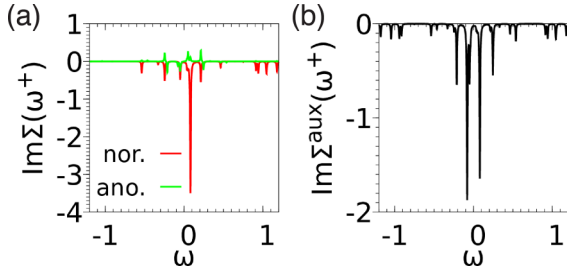
FIG. 1. (a), (b) Imaginary part of the real-frequency normal and anomalous (auxiliary) self-energy corresponding to an impurity system with s-wave pairing [Eq. (8)]. The parameters are $\epsilon_b = 0$, $V = 0.2$, $T = 0.1$, $U = 1.0$, $\Delta = 0.05$, $\mu = 0.5U - 0.4$, $\eta = 0.005$. The total filling of the system (impurity plus bath site) is 1.77, while half filling corresponds to 2.

FIG. 2. (a), (b) The imaginary part of the real-frequency normal and anomalous (auxiliary) self-energy at the X point for a d-wave SC solution of the Hubbard model, calculated within cellular DMFT with an ED impurity solver. The filling per site is 0.935 and the interaction is $U = 8$. The data of the normal and anomalous self-energy are reproduced from Fig. 4 of Ref. [44]. The solid (dashed) line shows the result much below (close to) T_c.

tral weight, and thus can be analytically continued with MaxEnt.

If the normalization of $A_\Sigma^{\mathrm{nor(aux)}}(\omega)$ can be determined by calculating static four-particle correlation functions [61], it is possible to perform MaxEnt directly on $\Sigma^{\mathrm{nor}}(i\omega_n)$ and $\Sigma^{\mathrm{aux}}(i\omega_n)$. Alternatively, one may define two auxiliary Green's functions for Σ^{aux} and Σ^{nor}, $\tilde{G}_{1(2),\mathbf{k}}^{\mathrm{aux}}(i\omega_n) = 1/(i\omega_n - [\Sigma_{\mathbf{k}}^{\mathrm{nor(aux)}}(i\omega_n) - \Sigma_{\mathbf{k},\infty}^{\mathrm{nor(aux)}}])$, respectively, with Σ_∞ the value of the self-energy in the high-frequency limit. Since $\tilde{G}_{1(2),\mathbf{k}}^{\mathrm{aux}}(i\omega_n)$ has positive definite spectral weight, we can perform a standard MaxEnt analytic continuation [54] and then apply the Kramers-Kronig transformation to get $\tilde{G}_{1(2),\mathbf{k}}^{\mathrm{aux}}(\omega + i\eta)$. We note that MaxEnt is not the only choice for the continuation of $\tilde{G}_{2,\mathbf{k}}^{\mathrm{aux}}(i\omega_n)$. All analytic continuation methods taking into account the positivity of the spectral weight can be used, including MaxEnt [54], sparse modeling [62,63], an artificial neural network approach [64] for numerical results with stochastic noise, and the Nevanlinna analytical continuation method [65]. Also the Padé approximation [28] can in principle be used if the stochastic noise is small enough. After this step, we can obtain the real-frequency self-energy as follows:

$$\Sigma_{\mathbf{k}}^{\mathrm{nor(aux)}}(\omega^+) = \omega^+ - \tilde{G}_{1(2),\mathbf{k}}^{\mathrm{aux}}(\omega^+)^{-1} + \Sigma_{\mathbf{k},\infty}^{\mathrm{nor(aux)}},$$

$$\Sigma_{\mathbf{k}}^{\mathrm{ano}}(\omega^+) = \Sigma_{\mathbf{k}}^{\mathrm{aux}}(\omega^+) - \frac{\Sigma_{\mathbf{k}}^{\mathrm{nor}}(\omega^+) - \Sigma_{\mathbf{k}}^{\mathrm{nor}}(-\omega^+)}{2}. \quad (7)$$

Benchmarks. In the following, we provide two benchmarks to verify that $A_\Sigma^{\mathrm{aux}}(\omega)$ is positive definite.

(1) Anderson model with s-wave pairing. Here, we consider an Anderson impurity model with a single bath site with s-wave pairing. The Hamiltonian is

$$H = U\hat{n}_{d\uparrow}\hat{n}_{d\downarrow} - \mu(\hat{n}_{d\uparrow} + \hat{n}_{d\downarrow}) + \epsilon_b c_\uparrow^\dagger c_\uparrow + \epsilon_b c_\downarrow^\dagger c_\downarrow$$
$$+ \Delta(c_\uparrow c_\downarrow + \mathrm{H.c.}) + (V d_\uparrow^\dagger c_\uparrow + V d_\downarrow^\dagger c_\downarrow + \mathrm{H.c.}), \quad (8)$$

with d the impurity operators and c the bath operators. U is the on-site interaction, μ the chemical potential, V the hybridization parameter, ϵ_b the bath energy level, and Δ the pair field. The real-frequency normal and anomalous Green's functions can be calculated using the Lehmann representation, with eigenstates and eigenenergies obtained by ED. The Dyson equation in the Nambu formalism then yields the self-energy. The real-frequency auxiliary self-energy is obtained according

to Eq. (5). As shown in Fig. 1, which corresponds to a system away from half filling, Im $\Sigma^{\mathrm{aux}}(\omega + i\eta)$ is negative for all real frequencies.

(2) d-wave pairing in the 2D Hubbard model. In the 2×2 cellular DMFT description with the ED impurity solver, the d-wave SC state of the single-band Hubbard model on the square lattice is mapped to a four-site cluster impurity model with, e.g., two bath orbitals coupled to each site [16,42,43,66,67]. The cluster Green's function in the Nambu formalism is diagonal in the four cluster momenta $\Gamma = (0, 0)$, $X = (\pi, 0)$, $Y = (0, \pi)$, and $M = (\pi, \pi)$. In the SC state, only the anomalous self-energies for X and Y are nonzero, and they are opposite in sign. We choose the X point and analyze the results from Ref. [44] for filling $n = 0.935$ per site in Fig. 2. As can be seen in Fig. 2(b), the spectral weight of the auxiliary self-energy $-\mathrm{Im}\,\Sigma^{\mathrm{aux}}(\omega^+)/\pi$ is positive.

Application to the superconducting state of K_3C_{60}. The alkali-doped fullerides A_3C_{60} (A = K, Rb, Cs) are strongly correlated electron systems which exhibit a SC dome next to a Mott insulating phase [68–76]. They are described by a three-band Hubbard model with an inverted Hund's coupling resulting from the overscreening of the small bare Hund's coupling by Jahn-Teller phonons [70,73,77]. The intraorbital spin-singlet SC state is unconventional, with a pairing glue originating from local orbital fluctuations, according to DMFT studies [4,15,78].

To the best of our knowledge, experimental ARPES results for the SC state of A_3C_{60} are lacking, possibly due to the strong air sensitivity of these compounds and the lack of good single crystals. We are also not aware of any calculated momentum-resolved electronic structures for the SC state of A_3C_{60}. The analytic continuation method presented in this Letter makes it possible to obtain the real-frequency anomalous self-energy, gap function and $A(\mathbf{k}, \omega)$.

Here, we focus on K_3C_{60} which is superconducting below $T_c \approx 18$ K [68]. The electronic structures are obtained within the framework of density functional theory (DFT) plus DMFT in the Nambu formalism (details of the method and parameters can be found in the SM [60]). The real-frequency $\Sigma^{\mathrm{nor}}(\omega)$ and $\Sigma^{\mathrm{ano}}(\omega)$ at $T = 10$ K in the SC state, obtained with the auxiliary analytic continuation method and the MaxEnt code of Ref. [83], are plotted in Fig. 3. As shown by the green curves,
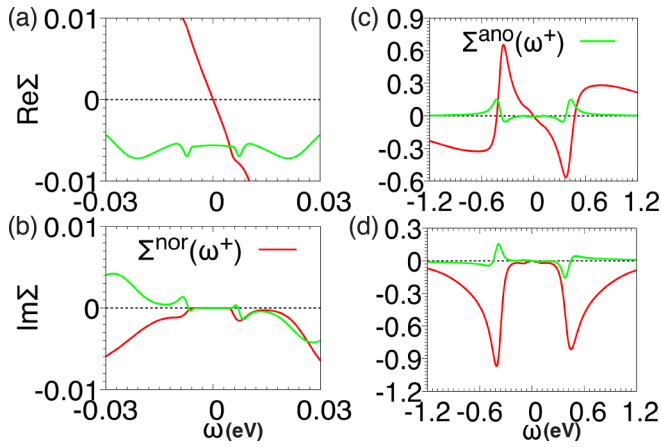
FIG. 3. The real-frequency $\Sigma^{nor}(\omega)$ and $\Sigma^{ano}(\omega)$ of K_3C_{60} at $T = 10$ K obtained by the auxiliary analytic continuation method. (a) and (b) [(c) and (d)] show the results on a smaller (larger) energy window. Re $\Sigma^{nor}(\omega)$ (red line) in (a) is shifted down by the Hartree-Fock value Re $\Sigma^{nor}_\infty = 1.82$ for a better visualization. The corresponding Matsubara frequency self-energies $\Sigma^{nor}(i\omega_n)$ and $\Sigma^{ano}(i\omega_n)$ are provided in the SM [60]. Here, we only show results for one of the degenerate t_{1u} orbitals.

$\Sigma^{ano}(\omega)$ features sign changes both in the real and imaginary parts. The corresponding $A(\mathbf{k}, \omega)$ is presented in Fig. 4. Figure 4(a) shows the results for $T = 10$ K ($< T_c \approx 18$ K), and Fig. 4(b) a zoom of the low-energy spectrum along the Γ-X path. We find a tiny SC gap with $\Delta_{sc} \approx 7.31/2 = 3.66$ meV, extracted at the half peak height [4] [Fig. 4(d)], which is slightly larger than the experimental value of 3.0 meV extracted from optical conductivity measurements [84]. The ratio $2\Delta_{sc}/k_B T_c \approx 4.71$ is in good agreement with the value recently extracted from Raman scattering in Ref. [85]. A $2\Delta_{sc}/k_B T_c$ ratio not much larger than the BCS result is consistent with the fact that K_3C_{60} is on the weak-coupling side of the SC dome [74].

As one can see from Fig. 4(b), faint spectral features exist inside the gap. This residual spectral weight leads to a partial filling in of the gap in the local spectral function, as seen in Fig. 4(d). It also contributes to the optical conductivity, which is consistent with the experimentally observed upturn in the real part of the optical conductivity in the energy range <5 meV, which grows as temperature is raised from $T = 6$ K to $T = T_c$ [84]. If T is increased above T_c, the gap disappears [see the spectrum for 30 K in Fig. 4(c)]. Furthermore, the bands broaden, which shows that the system becomes less coherent. Indeed, according to previous model studies, we expect the system to approach an orbital freezing crossover at even higher temperatures [15]. The $\mathbf{k}$-resolved spectra in a larger energy window, which also show the Hubbard bands, can be found in the SM [60].

Conclusions. We have addressed the problem of analytic continuation of the anomalous self-energy with nonpositive spectral weight. We introduced an auxiliary self-energy Σ^{aux}, which is a linear combination of the normal and
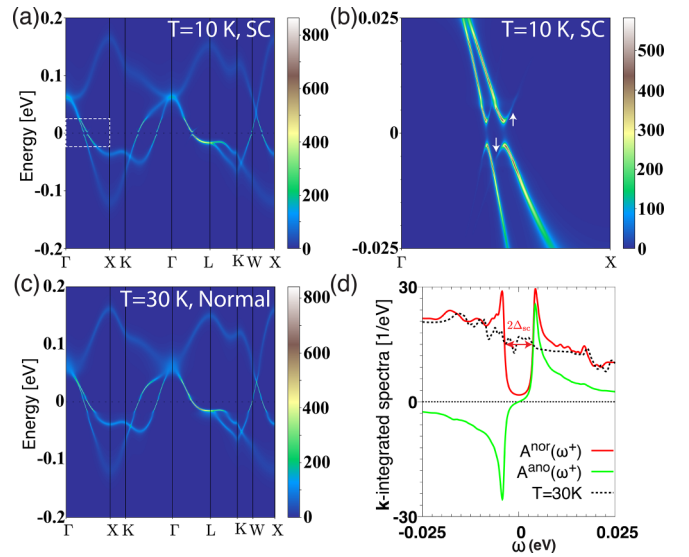
FIG. 4. Momentum-resolved spectral function $A(\mathbf{k}, \omega)$ of K_3C_{60}. (a) $A(\mathbf{k}, \omega)$ for the superconducting state at $T = 10$ K. (b) Zoom of the low-energy spectrum along Γ-X in the region marked by the white dashed box in (a). The white arrows highlight the back-bending of the Bogoliubov bands. (c) $A(\mathbf{k}, \omega)$ for the normal state at $T = 30$ K. (d) Low-energy structures of the $\mathbf{k}$-integrated normal and anomalous spectra $A^{nor(ano)}(\omega) = -\frac{1}{\pi} \text{Im} \frac{1}{N_\mathbf{k}} \sum_\mathbf{k} G^{nor(ano)}(\mathbf{k}, \omega)$.

anomalous self-energy, and showed both analytically and numerically that this function has positive definite spectral weight, regardless of the space-time or spin structure of the pairing state. This allows us to use the MaxEnt method to analytically continue Σ^{aux} from the Matsubara to the real-frequency axis and to extract the spectral weight of Σ^{ano}. Our method paves the way for systematic studies of the momentum-resolved electronic structures of conventional and unconventional superconductors. Access to the real-frequency anomalous self-energy makes it possible to calculate the gap function, spectral function, and optical conductivity, which are important for comparisons with experiments, and for revealing the pairing mechanism. We have demonstrated the usefulness of our approach by computing the spectral function of K_3C_{60} in the SC state. In the future, it will be interesting to extend these calculations to other types of superconductors, and in particular to the d-wave superconducting state of cuprates.

The data presented in this work can be downloaded from Ref. [86].

[1] L. P. Gor'kov, On the energy spectrum of superconductors, Sov. Phys. JETP **7**, 505 (1958).

[2] Y. Nambu, Quasi-particles and gauge invariance in the theory of superconductivity, Phys. Rev. **117**, 648 (1960).

[3] E. Gull and A. J. Millis, Pairing glue in the two-dimensional Hubbard model, Phys. Rev. B **90**, 041110(R) (2014).

[4] C. Yue, S. Hoshino, A. Koga, and P. Werner, Unconventional pairing from local orbital fluctuations in strongly correlated A_3C_{60}, Phys. Rev. B **104**, 075107 (2021).

[5] W. L. McMillan and J. M. Rowell, Lead phonon spectrum calculated from superconducting density of states, Phys. Rev. Lett. **14**, 108 (1965).

[6] J. P. Carbotte, Properties of boson-exchange superconductors, Rev. Mod. Phys. **62**, 1027 (1990).

[7] A. B. Migdal, Interaction between electrons and lattice vibrations in a normal metal, Sov. Phys. JETP **7**, 996 (1958).

[8] G. M. Eliashberg, Interactions between electrons and lattice vibrations in a superconductor, Sov. Phys. JETP **11**, 696 (1960).

[9] P. Morel and P. W. Anderson, Calculation of the superconducting state parameters with retarded electron-phonon interaction, Phys. Rev. **125**, 1263 (1962).

[10] A. V. Chubukov, A. Abanov, I. Esterlis, and S. A. Kivelson, Eliashberg theory of phonon-mediated superconductivity When it is valid and how it breaks down, Ann. Phys. **417**, 168190 (2020).

[11] F. Marsiglio, Eliashberg theory: A short review, Ann. Phys. **417**, 168102 (2020).

[12] D. J. Scalapino, Superconductivity and spin fluctuations, J. Low Temp. Phys. **117**, 179 (1999).

[13] S. Hoshino and P. Werner, Superconductivity from emerging magnetic moments, Phys. Rev. Lett. **115**, 247001 (2015).

[14] H. Kontani and S. Onari, Orbital-fluctuation-mediated superconductivity in iron pnictides: Analysis of the five-orbital Hubbard-Holstein model, Phys. Rev. Lett. **104**, 157001 (2010).

[15] S. Hoshino and P. Werner, Spontaneous orbital-selective Mott transitions and the Jahn-Teller metal of A_3C_{60}, Phys. Rev. Lett. **118**, 177002 (2017).

[16] B. Kyung, D. Sénéchal, and A.-M. S. Tremblay, Pairing dynamics in strongly correlated superconductivity, Phys. Rev. B **80**, 205109 (2009).

[17] T. A. Maier, D. Poilblanc, and D. J. Scalapino, Dynamics of the pairing interaction in the Hubbard and *t-J* models of high-temperature superconductors, Phys. Rev. Lett. **100**, 237001 (2008).

[18] T. Moriya and K. Ueda, Antiferromagnetic spin fluctuation and superconductivity, Rep. Prog. Phys. **66**, 1299 (2003).

[19] D. Poilblanc and D. J. Scalapino, Gap function $\phi(k, \omega)$ for a two-leg *t-J* ladder and the pairing interaction, Phys. Rev. B **71**, 174403 (2005).

[20] I. Giaever, H. R. Hart, Jr., and K. Megerle, Tunneling into superconductors at temperatures below 1°K, Phys. Rev. **126**, 941 (1962).

[21] J. M. Rowell, P. W. Anderson, and D. E. Thomas, Image of the phonon spectrum in the tunneling characteristic between superconductors, Phys. Rev. Lett. **10**, 334 (1963).

[22] J. M. Rowell, W. L. McMillan, and W. L. Feldmann, Superconductivity and lattice dynamics of white tin, Phys. Rev. B **3**, 4065 (1971).

[23] A. Damascelli, Z. Hussain, and Z.-X. Shen, Angle-resolved photoemission studies of the cuprate superconductors, Rev. Mod. Phys. **75**, 473 (2003).

[24] G. Liu, G. Wang, Y. Zhu, H. Zhang, G. Zhang, X. Wang, Y. Zhou, W. Zhang, H. Liu, L. Zhao, J. Meng, X. Dong, C. Chen, Z. Xu, and X. J. Zhou, Development of a vacuum ultraviolet

[25] J. Shi, S.-J. Tang, B. Wu, P. T. Sprunger, W. L. Yang, V. Brouet, X. J. Zhou, Z. Hussain, Z.-X. Shen, Z. Zhang, and E. W. Plummer, Direct extraction of the Eliashberg function for electron-phonon coupling: A case study of Be(10$\bar{1}$0), Phys. Rev. Lett. **92**, 186401 (2004).

[26] J. M. Bok, J. J. Bae, H.-Y. Choi, C. M. Varma, W. Zhang, J. He, Y. Zhang, L. Yu, and X. J. Zhou, Quantitative determination of pairing interactions for high-temperature superconductivity in cuprates, Sci. Adv. **2**, e1501329 (2016).

[27] Y. Yamaji, T. Yoshida, A. Fujimori, and M. Imada, Hidden self-energies as origin of cuprate superconductivity revealed by machine learning, Phys. Rev. Res. **3**, 043099 (2021).

[28] H. J. Vidberg and J. W. Serene, Solving the Eliashberg equations by means of *N*-point Padé approximants, J. Low Temp. Phys. **29**, 179 (1977).

[29] W. Metzner and D. Vollhardt, Correlated lattice fermions in $d = \infty$ dimensions, Phys. Rev. Lett. **62**, 324 (1989).

[30] A. Georges and G. Kotliar, Hubbard model in infinite dimensions, Phys. Rev. B **45**, 6479 (1992).

[31] M. Jarrell, Hubbard model in infinite dimensions: A quantum Monte Carlo study, Phys. Rev. Lett. **69**, 168 (1992).

[32] A. Georges, G. Kotliar, W. Krauth, and M. J. Rozenberg, Dynamical mean-field theory of strongly correlated fermion systems and the limit of infinite dimensions, Rev. Mod. Phys. **68**, 13 (1996).

[33] G. Kotliar, S. Y. Savrasov, K. Haule, V. S. Oudovenko, O. Parcollet, and C. A. Marianetti, Electronic structure calculations with dynamical mean-field theory, Rev. Mod. Phys. **78**, 865 (2006).

[34] M. H. Hettler, A. N. Tahvildar-Zadeh, M. Jarrell, T. Pruschke, and H. R. Krishnamurthy, Nonlocal dynamical correlations of strongly interacting electron systems, Phys. Rev. B **58**, R7475 (1998).

[35] M. H. Hettler, M. Mukherjee, M. Jarrell, and H. R. Krishnamurthy, Dynamical cluster approximation: Nonlocal dynamics of correlated electron systems, Phys. Rev. B **61**, 12739 (2000).

[36] K. Aryanpour, M. H. Hettler, and M. Jarrell, Analysis of the dynamical cluster approximation for the Hubbard model, Phys. Rev. B **65**, 153102 (2002).

[37] T. A. Maier, M. Jarrell, T. Prushke, and M. Hettler, Quantum cluster theories, Rev. Mod. Phys. **77**, 1027 (2005).

[38] A. I. Lichtenstein and M. I. Katsnelson, Antiferromagnetism and *d*-wave superconductivity in cuprates: A cluster dynamical mean-field theory, Phys. Rev. B **62**, R9283 (2000).

[39] G. Kotliar, S. Y. Savrasov, G. Pálsson, and G. Biroli, Cellular dynamical mean field approach to strongly correlated systems, Phys. Rev. Lett. **87**, 186401 (2001).

[40] A. Liebsch, H. Ishida, and J. Merino, Multisite versus multiorbital Coulomb correlations studied within finite-temperature exact diagonalization dynamical mean-field theory, Phys. Rev. B **78**, 165123 (2008).

[41] M. Caffarel and W. Krauth, Exact diagonalization approach to correlated fermions in infinite dimensions: Mott transition and superconductivity, Phys. Rev. Lett. **72**, 1545 (1994).

[42] A. Foley, S. Verret, A.-M. S. Tremblay, and D. Sénéchal, Coexistence of superconductivity and antiferromagnetism in

the Hubbard model for cuprates, Phys. Rev. B **99**, 184510 (2019).

[43] S. Sakai, M. Civelli, and M. Imada, Hidden fermionic excitation boosting high-temperature superconductivity in cuprates, Phys. Rev. Lett. **116**, 057003 (2016).

[44] S. Sakai, M. Civelli, and M. Imada, Hidden-fermion representation of self-energy in pseudogap and superconducting states of the two-dimensional Hubbard model, Phys. Rev. B **94**, 115130 (2016).

[45] S. Sakai, M. Civelli, and M. Imada, Direct connection between Mott insulators and *d*-wave high-temperature superconductors revealed by continuous evolution of self-energy poles, Phys. Rev. B **98**, 195109 (2018).

[46] A. Georges, G. Kotliar, and W. Krauth, Superconductivity in the two-band Hubbard model in infinite dimensions, Z. Phys. B **92**, 313 (1993).

[47] K. Haule, Quantum Monte Carlo impurity solver for cluster dynamical mean-field theory and electronic structure calculations with adjustable cluster base, Phys. Rev. B **75**, 155113 (2007).

[48] A. Koga and P. Werner, Polarized superfluidity in the imbalanced attractive Hubbard model, J. Phys. Soc. Jpn. **79**, 064401 (2010).

[49] M. Sentef, P. Werner, E. Gull, and A. P. Kampf, Superconducting phase and pairing fluctuations in the half-filled two-dimensional Hubbard model, Phys. Rev. Lett. **107**, 126401 (2011).

[50] G. Sordi, P. Sémon, K. Haule, and A.-M. S. Tremblay, Strong coupling superconductivity, pseudogap, and Mott transition, Phys. Rev. Lett. **108**, 216401 (2012).

[51] E. Gull and A. J. Millis, Superconducting and pseudogap effects on the interplane conductivity and Raman scattering cross section in the two-dimensional Hubbard model, Phys. Rev. B **88**, 075127 (2013).

[52] P. Sémon, G. Sordi, and A.-M. S. Tremblay, Ergodicity of the hybridization-expansion Monte Carlo algorithm for broken-symmetry states, Phys. Rev. B **89**, 165113 (2014).

[53] C. Yue, H. Aoki, and P. Werner, Superconductivity enhanced by pair fluctuations between wide and narrow bands, Phys. Rev. B **106**, L180506 (2022).

[54] M. Jarrell and J. Gubernatis, Bayesian inference and the analytic continuation of imaginary-time quantum Monte Carlo data, Phys. Rep. **269**, 133 (1996).

[55] E. Gull, O. Parcollet, and A. J. Millis, Superconductivity and the pseudogap in the two-dimensional Hubbard model, Phys. Rev. Lett. **110**, 216405 (2013).

[56] A. Reymbaut, D. Bergeron, and A.-M. S. Tremblay, Maximum entropy analytic continuation for spectral functions with nonpositive spectral weight, Phys. Rev. B **92**, 060509(R) (2015).

[57] K. Balzer and M. Eckstein, Auxiliary Hamiltonian representation of the nonequilibrium Dyson equation, Phys. Rev. B **89**, 035148 (2014).

[58] K. Balzer, The auxiliary Hamiltonian approach and its generalization to non-local self-energies, J. Phys.: Conf. Ser. **696**, 012001 (2016).

[59] K. Seki and S. Yunoki, Brillouin-zone integration scheme for many-body density of states: Tetrahedron method combined with cluster perturbation theory, Phys. Rev. B **93**, 245115 (2016).

[60] See Supplemental Material at http://link.aps.org/supplemental/10.1103/PhysRevB.108.L220503 for a proof of the positiveness of the spectral weight of Σ^{aux}, and for additional numerical data, which includes Refs. [32,33,52,53,72,73,79–82].

[61] X. Wang, H. T. Dang, and A. J. Millis, High-frequency asymptotic behavior of self-energies in quantum impurity models, Phys. Rev. B **84**, 073104 (2011).

[62] J. Otsuki, M. Ohzeki, H. Shinaoka, and K. Yoshimi, Sparse modeling approach to analytical continuation of imaginary-time quantum Monte Carlo data, Phys. Rev. E **95**, 061302(R) (2017).

[63] K. Yoshimi, J. Otsuki, Y. Motoyama, M. Ohzeki, and H. Shinaoka, SpM: Sparse modeling tool for analytic continuation of imaginary-time Green's function, Comput. Phys. Commun. **244**, 319 (2019).

[64] R. Fournier, L. Wang, O. V. Yazyev, and Q. Wu, Artificial neural network approach to the analytic continuation problem, Phys. Rev. Lett. **124**, 056401 (2020).

[65] J. Fei, C.-N. Yeh, and E. Gull, Nevanlinna analytical continuation, Phys. Rev. Lett. **126**, 056402 (2021).

[66] S. S. Kancharla, B. Kyung, D. Sénéchal, M. Civelli, M. Capone, G. Kotliar, and A.-M. S. Tremblay, Anomalous superconductivity and its competition with antiferromagnetism in doped Mott insulators, Phys. Rev. B **77**, 184516 (2008).

[67] M. Civelli, Doping-driven evolution of the superconducting state from a doped Mott insulator: Cluster dynamical mean-field theory, Phys. Rev. B **79**, 195113 (2009).

[68] A. F. Hebard, M. J. Rosseinsky, R. C. Haddon, D. W. Murphy, S. H. Glarum, T. T. M. Palstra, A. P. Ramirez, and A. R. Kortan, Superconductivity at 18 K in potassium-doped C_{60}, Nature (London) **350**, 600 (1991).

[69] J. E. Han, O. Gunnarsson, and V. H. Crespi, Strong superconductivity with local Jahn-Teller phonons in C_{60} solids, Phys. Rev. Lett. **90**, 167006 (2003).

[70] M. Capone, M. Fabrizio, C. Castellani, and E. Tosatti, Strongly correlated superconductivity, Science **296**, 2364 (2002).

[71] M. Capone, M. Fabrizio, C. Castellani, and E. Tosatti, Colloquium: Modeling the unconventional superconducting properties of expanded A_3C_{60} fullerides, Rev. Mod. Phys. **81**, 943 (2009).

[72] Y. Nomura, K. Nakamura, and R. Arita, *Ab initio* derivation of electronic low-energy models for C_{60} and aromatic compounds, Phys. Rev. B **85**, 155452 (2012).

[73] Y. Nomura, S. Sakai, M. Capone, and R. Arita, Unified understanding of superconductivity and Mott transition in alkali-doped fullerides from first principles, Sci. Adv. **1**, e1500568 (2015).

[74] R. H. Zadik, Y. Takabayashi, G. Klupp, R.-H. Colman, A.-Y. Ganin, A. Potonik, P. Jegli, D. Aron, P. Matus, K. Kamarás *et al.*, Optimized unconventional superconductivity in a molecular Jahn-Teller metal, Sci. Adv. **1**, e1500059 (2015).

[75] Y. Nomura, S. Sakai, M. Capone, and R. Arita, Exotic *s*-wave superconductivity in alkali-doped fullerides, J. Phys.: Condens. Matter **28**, 153001 (2016).

[76] Y. Takabayashi and K. Prassides, Unconventional high-T_c superconductivity in fullerides, Phil. Trans. R. Soc. A **374**, 20150320 (2016).

[77] M. Fabrizio and E. Tosatti, Nonmagnetic molecular Jahn-Teller Mott insulators, Phys. Rev. B **55**, 13465 (1997).

[78] K. Steiner, S. Hoshino, Y. Nomura, and P. Werner, Long-range orders and spin/orbital freezing in the two-band Hubbard model, Phys. Rev. B **94**, 075107 (2016).

[79] F. Aryasetiawan, M. Imada, A. Georges, G. Kotliar, S. Biermann, and A. I. Lichtenstein, Frequency-dependent local interactions and low-energy effective models from electronic structure calculations, Phys. Rev. B **70**, 195104 (2004).

[80] Y. Nomura and R. Arita, *Ab initio* downfolding for electron-phonon-coupled systems: Constrained density-functional perturbation theory, Phys. Rev. B **92**, 245108 (2015).

[81] P. Werner, A. Comanac, L. de' Medici, M. Troyer, and A. J. Millis, Continuous-time solver for quantum impurity models, Phys. Rev. Lett. **97**, 076405 (2006).

[82] E. Gull, A. J. Millis, A. I. Lichtenstein, A. N. Rubtsov, M. Troyer, and P. Werner, Continuous-time Monte Carlo methods for quantum impurity models, Rev. Mod. Phys. **83**, 349 (2011).

[83] R. Levy, J. P. F. LeBlanc, and E. Gull, Implementation of the maximum entropy method for analytic continuation, Comput. Phys. Commun. **215**, 149 (2017).

[84] L. Degiorgi, G. Briceno, M. S. Fuhrer, A. Zettl, and P. Wachter, Optical measurements of the superconducting gap in single-crystal K_3C_{60} and Rb_3C_{60}, Nature (London) **369**, 541 (1994).

[85] R.-S. Wang, D. Peng, L.-N. Zong, Z.-W. Zhu, and X.-J. Chen, Full set of superconducting parameters of K_3C_{60}, Carbon **202**, 325 (2023).

[86] https://doi.org/10.5281/zenodo.7779381.

[87] L. Huang, Y. Wang, Z. Y. Meng, L. Du, P. Werner, and X. Dai, iQIST: An open source continuous-time quantum Monte Carlo impurity solver toolkit, Comput. Phys. Commun. **195**, 140 (2015).

[88] L. Huang, iQIST v0.7: An open source continuous-time quantum Monte Carlo impurity solver toolkit, Comput. Phys. Commun. **221**, 423 (2017).